Point defects, impurities, and small hole polarons in GdTiO₃

L. Bjaalie,[1] A. Janotti,[1,*] K. Krishnaswamy,[2] and C. G. Van de Walle[1]

[1]*Materials Department, University of California, Santa Barbara, California 93106-5050, USA*
[2]*Department of Electrical and Computer Engineering, University of California, Santa Barbara, California 93106-9560, USA*

The electronic structure of native defects and impurities in GdTiO₃, a rare-earth titanate Mott insulator, is studied using density functional theory with a hybrid functional. Among native defects, the cation vacancies have the lowest formation energies in oxygen-rich conditions and oxygen vacancies have the lowest formation energy in oxygen-poor conditions. Among the impurities, Sr_{Gd}, H_i, and C_O have low formation energies. A common feature of the native defects and impurities is that they lead to the formation of small hole polarons, which explains the frequent observation of *p*-type hopping conductivity in the rare-earth titanates. These small hole polarons also lead to optical absorption and act as electron traps in devices.

I. INTRODUCTION

The rare-earth titanates (RTiO₃, where R is a trivalent rare-earth ion), are prototypical Mott insulators [1,2], with a $3d^1$ electron configuration (Ti^{3+}). The energy gap arises from strong intra-atomic Coulomb electron-electron interactions that split the partially filled d band, separating an occupied lower Hubbard band (LHB) from an unoccupied upper Hubbard band (UHB) [3]. In practice, this means that both the valence band (LHB) and conduction band (UHB) are made up of Ti $3d$ states. These compounds form in the perovskite structure, with appreciable octahedral distortions. The titanates, and GdTiO₃ (GTO) in particular, have recently attracted a great deal of attention because of the ability to form a two-dimensional electron gas (2DEG) at the interface with a nonpolar oxide such as SrTiO₃ (STO) [4], allowing the study of interaction-induced phenomena in an electron liquid with unprecedentedly high density and opening the way to novel device applications [5].

Understanding and controlling the electronic properties of these materials is still a challenge. Bulk powder samples are reported to be *p*-type [2,6], with thermally activated transport attributed to small polaron hopping [2]. Similar hopping conductivity is found in GTO thin films grown by molecular beam epitaxy (MBE) [7]. One goal of the present study is to investigate the origin of these small polarons. The presence of acceptor-type dopants could explain the *p*-type conductivity, and we investigate the likelihood of various impurities being incorporated, and their effect on the electronic structure. In addition, we present a comprehensive study of native point defects (vacancies, interstitials, and antisites). In general, such defects introduce states that affect electronic and optical properties by acting as carrier traps or recombination centers. Surprisingly, we find that in the rare-earth titanates *all* the native defects act as a source of polarons, including oxygen vacancies. We identify which point defects are most likely to form, how they would affect the conductivity, and how they impact other electronic and optical properties.

Details of our approach are given in Sec. II. We use density functional theory (DFT) with a hybrid functional, which not only provides reliable values for defect formation energies and transition levels in semiconductors and insulators [8–12], but also accurately describes localization phenomena (essential for polarons) as well as the insulating nature of perovskite Mott insulators [13,14]. Electronic and structural properties of an array of native defects are described in Sec. III. In addition to the native defects, in Sec. IV we investigate C, Sr, and H impurities, which are likely to be present during growth of GTO on STO. Section V, finally, discusses the impact of defects on conductivity, optical properties, and electronic devices.

II. METHOD

A. Density functional theory

The calculations are based on density functional theory (DFT) using the screened hybrid functional of Heyd-Scuseria-Ernzerhof (HSE06) [15,16], implemented with the projector augmented wave method in VASP [17,18]. The HSE06 functional provides partial cancellation of self-interaction and has been shown to give an accurate description of the electronic and structural properties of a wide range of materials [19,20]. It also describes Mott insulating behavior, which results from strong electronic correlation, as it yields an accurate description of electron localization [13]. The mixing parameter was set to the standard value of 0.25. All calculations include spin polarization, essential to correctly describe GTO as a Mott insulator.

GTO assumes a distorted orthorhombic ($Pnmb$) structure, with a 20-atom unit cell. The calculated lattice parameters and bond angles are in good agreement with experiment, and the value of the energy gap is 2.02 eV, in agreement with optical measurements [21]. Figure 1 shows the relative positions of the O $2p$ band and the lower and upper Hubbard bands. Defect calculations were performed in a 160-atom $2 \times 2 \times 2$ supercell. Wave functions were expanded in a plane-wave basis set with a 400 eV energy cutoff, and the $(1/4,1/4,1/4)$ special k point was used for integrations over the Brillouin zone. Atomic structure was considered converged when Hellman-Feynman forces were less than 0.01 eV/Å. Symmetry breaking was explicitly allowed by choosing low-symmetry initial structural configurations.

---

*Current address: Materials Science and Engineering, University of Delaware, Newark, Delaware 19716-3106, USA.
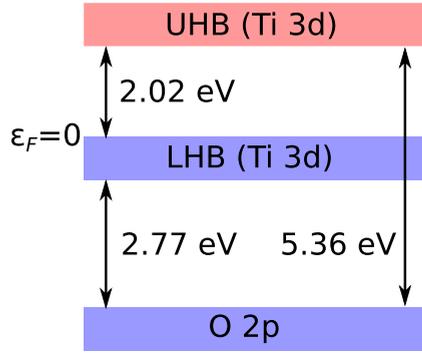
FIG. 1. Schematic band structure of GdTiO₃. The zero of the Fermi level is referenced to the top of the lower Hubbard band (LHB). The gap is between the lower and upper Hubbard band (UHB).

TABLE I. Calculated and experimental formation enthalpies.

Material	Present work (eV)	Experiment (eV)
GdTiO₃	−17.22	
TiO₂	−9.13	−9.74[a]
Gd₂O₃	−18.67	−18.80[b]
Gd₂Ti₂O₇	−38.05	−39.62[c]
H₂O	−2.68	−2.51[b]
CO₂	−3.89	−4.07[b]
SrO	−5.64	−6.12[a]
SrTiO₃	−16.05	−17.14[d]

[a]Reference [25].
[b]Reference [26].
[c]Reference [27].
[d]Reference [28].

B. Formation energy and transition levels

The formation energy of a defect D in a charge state q is defined as [22]:

$$E^f(D^q) = E_{\text{tot}}(D^q) - E_{\text{tot}} - \sum_i n_i \mu_i + q\epsilon_F + \Delta^q, \quad (1)$$

where $E_{\text{tot}}(D^q)$ is the total energy of a supercell containing a defect D in charge state q, and E_{tot} is the total energy of the perfect GTO supercell. n_i is the number of atoms of species i ($i = $ Gd, Ti, O, Sr, H, or C) added to ($n_i > 0$) and/or removed from ($n_i < 0$) the perfect crystal to form the defect, and μ_i are the atomic chemical potentials. ϵ_F is the Fermi level referenced to the valence-band maximum (VBM) (for GTO, the top of the LHB). Δ^q is a correction term to align the electrostatic potential in the perfect bulk and defect supercells and to account for finite-cell size effects on the total energies of charged defects, using the approach of Freysoldt *et al.* [23,24].

The charge-state transition level (q/q') is defined as the Fermi-level position below which the defect is most stable in charge state q and above which the defect is most stable in charge state q'. It can be derived from the formation energies:

$$(q/q') = \frac{E^f(D^q; \epsilon_F = 0) - E^f(D^{q'}; \epsilon_F = 0)}{(q' - q)}, \quad (2)$$

where $E_f(D^q; \epsilon_F = 0)$ is the defect formation energy for charge state q when ϵ_F is at the top of the LHB. The position of the transition level in the gap is independent of the choice of chemical potentials.

C. Atomic chemical potentials

The defect formation energies depend on the atomic chemical potentials μ_i, which are taken with respect to the total energy per atom of the standard phase of the species i, i.e., μ_{Gd} is referenced to the total energy per atom of Gd metal (hcp), and μ_H to half of the total energy of an isolated H₂ molecule. The chemical potentials are variables, but restricted by the formation of limiting phases containing the relevant species. The chemical potentials must satisfy the stability condition of GTO:

$$\mu_{Gd} + \mu_{Ti} + 3\mu_O = \Delta H_f(\text{GTO}), \quad (3)$$

with $\mu_{Gd} \leqslant 0$, $\mu_{Ti} \leqslant 0$, and $\mu_O \leqslant 0$, and $\Delta H_f(\text{GTO})$ the formation enthalpy.

The chemical potentials are further restricted by the formation of TiO₂, Gd₂O₃, and Gd₂Ti₂O₇ phases:

$$\mu_{Ti} + 2\mu_O \leqslant \Delta H_f(\text{TiO}_2), \quad (4)$$

$$2\mu_{Gd} + 3\mu_O \leqslant \Delta H_f(\text{Gd}_2\text{O}_3), \text{ and} \quad (5)$$

$$2\mu_{Gd} + 2\mu_{Ti} + 7\mu_O \leqslant \Delta H_f(\text{Gd}_2\text{Ti}_2\text{O}_7), \quad (6)$$

Calculated and experimental formation enthalpies are listed in Table I. By using Eqs. (3)–(6) we can define a region in the μ_O vs μ_{Ti} plane in which GTO is stable, as shown in Fig. 2.

For calculating the formation energies we focus on two extreme cases, indicated with filled black circles in Fig. 2. The first is defined by Gd₂Ti₂O₇ (pyrochlore) as the limiting phase, with $\mu_O = -3.61$ eV; since this sets an upper limit on μ_O we refer to this as "oxygen-rich," though it should be noted that the value of μ_O is quite low. While this does not strictly
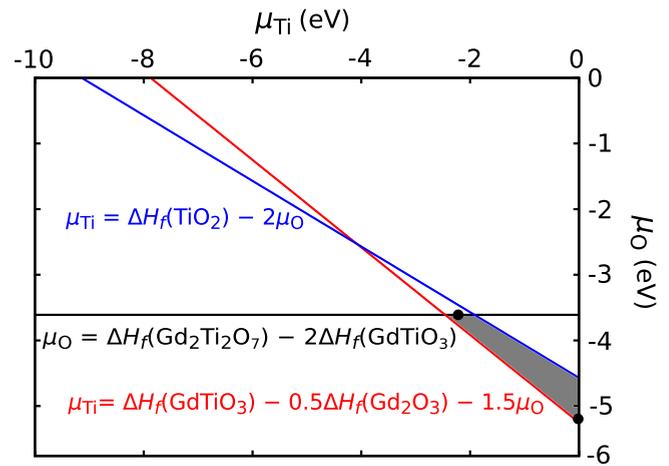
FIG. 2. Allowed values of O and Ti chemical potentials (gray shaded region) defining the stability of GdTiO₃. The chemical potentials μ_{Ti}, μ_O, and μ_{Gd} are limited by the formation of secondary phases TiO₂ (rutile), Gd₂O₃, and Gd₂Ti₂O₇. The filled black circles correspond to $\mu_O = -3.61$ eV and $\mu_O = -5.25$ eV, spanning the range of possible values of μ_O.
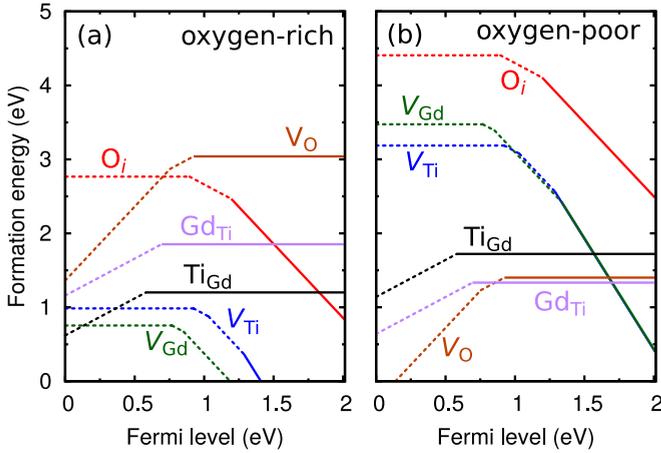
FIG. 3. Formation energies as a function of Fermi level for native defects in GTO under (a) oxygen-rich and (b) oxygen-poor conditions. The slopes of the lines indicate the charge state of the defect, and the kinks in the lines correspond to the position of the charge-state transition levels in the gap [Eq. (2)]. The dotted lines indicate charge states corresponding to hole polarons bound to the defect center.

specify the value of μ_{Ti}, the stability region is sufficiently narrow that μ_{Ti} can vary by only 0.55 eV, and we chose a value at the center of this region: $\mu_{Ti} = -2.20$ eV. "Oxygen-poor" conditions correspond to Gd_2O_3 as the limiting phase, with $\mu_O = -5.25$ eV and $\mu_{Ti} = 0$ eV.

When considering impurity atoms, we also need to take into account limiting phases for H, C, and Sr; these are also included in Table I. μ_H is subject to the constraint $2\mu_H + \mu_O \leqslant \Delta H_f(H_2O)$, but due to the low values of μ_O needed to stabilize GTO, H_2O turns out not to be a limiting phase. Similarly for C, CO_2 is not a limiting phase. For Sr, SrO, and $SrTiO_3$ are possible limiting phases. We find that for our choice of oxygen-rich conditions, $SrTiO_3$ limits μ_{Sr} to -3.02 eV, and for oxygen-poor conditions, SrO limits μ_{Sr} to -0.39 eV.

III. RESULTS: NATIVE DEFECTS

The formation energies of all native defects considered in our study are shown in Fig. 3. The intrinsic defects include vacancies (V_{Gd}, V_{Ti}, and V_O), antisites (Ti_{Gd} and Gd_{Ti}), oxygen interstitials (O_i), and cation interstitials (Ti_i and Gd_i). The cation interstitials are found to have high formation energies (due to the highly compact perovskite structure and their large atomic radius) and a discussion of their behavior is not included.

A. Polarons in bulk GdTiO₃

We have previously studied small hole polarons in bulk GTO [29]. In GTO, Ti atoms are in a Ti^{3+} configuration. Removing an electron leads to a hole in the LHB, which localizes in the form of a small polaron, corresponding to a single Ti^{4+}. The Ti-O bonds surrounding this Ti^{4+} atom shrink relative to the bulk bond lengths. Such small polarons are stable in bulk GTO with a self-trapping energy of 0.55 eV; i.e., the localized state is 0.55 eV lower in energy than the delocalized state of the hole (at the top of the LHB). Within a
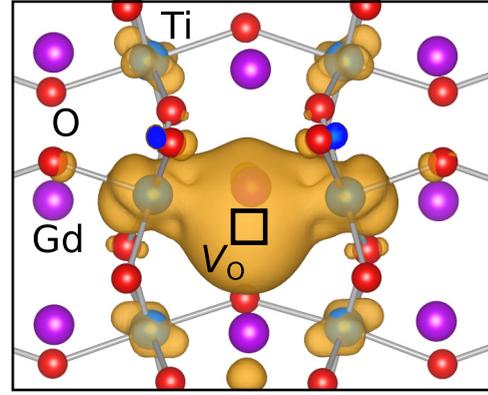
FIG. 4. Charge density for the Ti-Ti bonding state in an oxygen vacancy (V_O), with isosurface set to 10% of the maximum.

defect model, this corresponds to a $(+1/0)$ transition level at 0.55 eV above the VBM (top of the LHB).

B. Oxygen vacancies

As expected, the formation energy of V_O in GTO is low for oxygen-poor conditions [Fig. 3(b)]. Oxygen is twofold coordinated, and the removal of an oxygen atom leaves two Ti $3d$ "dangling bonds." These dangling bonds form an occupied bonding state resonant in the LHB (Fig. 4) and an empty antibonding state resonant in the UHB. In the neutral charge state, the Ti-Ti distance is 3.69 Å (compared to 3.81Å in bulk GTO), and the bonding state is doubly occupied.

This atomic and electronic structure is similar to what is found for V_O in other perovskite oxides such as STO [30], $SrZrO_3$ [31], or $LaAlO_3$ [32]. Those other oxides are band insulators, however, and the bonding state is located within the band gap of the oxide; $+1$ and $+2$ charge states can then be stabilized by taking electrons out of this state. In contrast, in GTO the bonding state overlaps with the LHB and hence removing electrons from this state corresponds to inducing holes in the LHB. These holes stabilize in the form of one or two small polarons localized on the Ti atoms neighboring the vacancy, while the Ti-Ti bonding state itself remains doubly occupied. The structure of these polarons is similar to that of bulk polarons [29], and the structure of the "center" of the defect remains very similar to that of the neutral charge state.

The neutral charge state is therefore in principle the only "stable" charge state of the defect, within the traditional view of defects in semiconductors and insulators [22]. To indicate that the $+1$ and $+2$ charge states correspond to polarons bound to the neutral defect center, we show the corresponding formation energies in dotted lines in Fig. 3. The $(+2/+1)$ transition level occurs at 0.75 eV and $(+1/0)$ at 0.92 eV. Since in the bulk a hole polaron is stabilized by 0.55 eV compared to a free hole, as discussed in Sec. III A, the values indicate that the first polaron is bound to the defect center by 0.37 eV, and the second by 0.20 eV.

C. Cation vacancies

Gd and Ti both have valence 3 in GTO; removing either a Gd or Ti therefore leads to a deficiency of three electrons (in the neutral charge state of the defect). One expects the
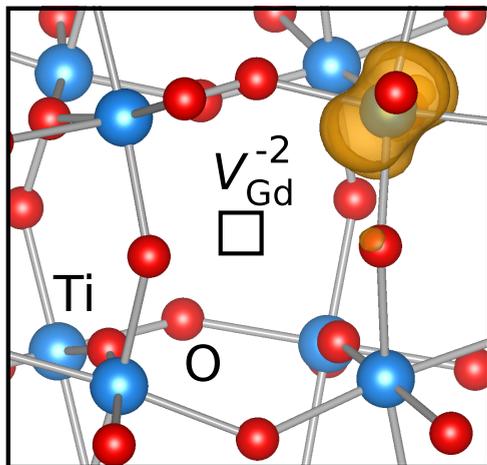
FIG. 5. Formation of a single small hole polaron for V_{Gd}^{-2}. The charge-density isosurface illustrating the wave function of the polaron state is set to 10% of the maximum value.

FIG. 6. Formation energies as a function of Fermi level for impurities in GTO under (a) oxygen-rich and (b) oxygen-poor conditions. The dotted lines indicate charge states corresponding to hole polarons bound to the impurity.

most stable charge state of these defects to be the -3 charge state, in which these electrons are added back into the lattice; this is indeed reflected in the low formation energy of this charge state, at least when the Fermi level is high (Fig. 3). The occupied bonding states corresponding to the -3 charge state are located well below the top of the LHB, and hence changing the charge state to -2, -1, or neutral requires taking electrons from states within the LHB; these missing electrons then manifest themselves in the form of small hole polarons on nearby Ti atoms. Figure 5 illustrates the situation for the $q = -2$ charge state of V_{Gd}, in which a single polaron is located adjacent to the vacancy. The -1 charge state has two polarons, and the neutral charge state has three.

In the -3 charge state of V_{Ti} (no polarons) the O atoms with a missing Ti neighbor shorten their remaining Ti-O bond, and the nearby Gd atoms displace inwards towards the vacancy. For V_{Gd} the predominant change in atomic structure is in the increase in bond angles of the Ti and O atoms surrounding the Gd vacancy.

The formation energies for all charge states are shown in Fig. 3; as expected, they are lowest under oxygen-poor conditions. Cation vacancies act as deep acceptors. V_{Ti} has transition levels at 0.92 eV ($0/-1$), 1.03 eV ($-1/-2$), and 1.29 eV ($-2/-3$), and V_{Gd} at 0.77 eV ($0/-1$), 0.85 eV ($-1/-2$), and 1.34 eV ($-2/-3$). The binding energy of the polarons to the defect center is clearly larger than it was for binding to a neutral oxygen vacancy, which can be attributed to the defect center now being triply negatively charged rather than neutral.

D. Antisites

Ti_{Gd} and Gd_{Ti} antisites have moderately low formation energies for both oxygen-rich and oxygen-poor conditions [Figs. 3(a) and 3(b)]. Ti has four valence electrons, and therefore one more electron than the Gd atom which it replaces (which transfers its electrons to low-lying oxygen states). This extra electron is localized on the Ti atom, as for a Ti atom in bulk GTO, but with the electron in a state 0.38 eV below the LHB. We therefore expect the Ti_{Gd} defect to be stable in a
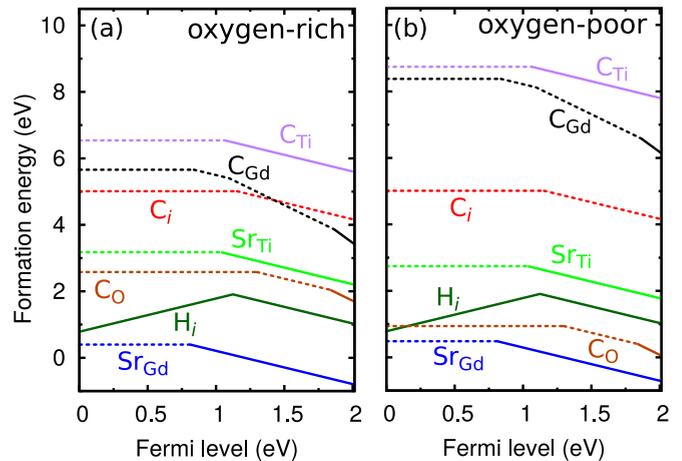
neutral charge state, which is indeed the case over most of the range of Fermi levels. However, a hole polaron can occur in the vicinity of the defect, which effectively gives the appearance of the $+1$ charge state being stabilized when the Fermi level is below the $(+1/0)$ transition level at 0.58 eV. The similarity of this transition-level value to the value of 0.55 eV for the bulk polaron indicates the interaction between the polaron and the Ti_{Gd} defect is quite weak, with a binding energy of only 0.03 eV.

For the case of Gd_{Ti} there is now a missing electron, and the number of LHBs is reduced by one. Again the defect is most stable in a neutral charge state, but a small polaron can be formed in the vicinity, seemingly stabilizing a $q = +1$ charge state with a $(+1/0)$ transition level at 0.69 eV (corresponding to a binding energy for the polaron of 0.14 eV).

E. Oxygen interstitials

The oxygen interstitial is stable in an asymmetric dumbbell configuration for all charge states ($0, -1$ and -2). The adjacent O host atom is displaced, and the Ti-O-Ti bond angles for both O atoms are strongly distorted. The interstitial bonds to two Ti atoms and introduces two Ti-O bonding states 0.75 eV above the O $2p$ band. The -2 charge state is the "natural" charge state for this defect. Forming a -1 or 0 charge state requires removing electrons, which need to be taken from the LHB, thus leading to the formation of one or two hole polarons; the transition levels are at 0.89 eV ($0/+1$) and 1.20 eV ($+1/+2$). Oxygen interstitials have higher formation energies than the other defects considered here (Fig. 3), meaning that they are not likely to form.

IV. RESULTS: IMPURITIES

The formation energies of impurities considered in our study are shown in Fig. 6. We studied Sr substitutional impurities (Sr_{Gd}), H interstitials (H_i), and carbon-related defects: carbon interstitials (C_i), and substitutional C on Gd (C_{Gd}), Ti (C_{Ti}), and O sites (C_O). All these elements are candidates for unintentional doping that may occur during

growth. H and C are ubiquitious impurities, and in particular are part of the metallorganic precursors used in hybrid MBE [7]. Sr is present during the growth of STO/GTO interfaces, and has also been used in intentional doping of GTO [29,33–35].

A. Strontium

The calculated formation energy of Sr on a Gd site (Sr_{Gd}) is very low (Fig. 6). Indeed, experimentally it is straightforward to dope GTO with Sr [29] or form $Gd_{1-x}Sr_xTiO_3$ alloys [33,35]. The atomic structure of Sr_{Gd} is similar to that of the Gd vacancy: the bond angles of the surrounding Ti and O atoms increase slightly. As expected from the 2+ valence of Sr (compared to 3+ for Gd), the impurity acts as an acceptor: over most of the range of Fermi levels it occurs in a −1 charge state, and a (−1/0) transition level occurs at 0.81 eV. The neutral charge state is characterized by a small hole polaron on a neighboring Ti atom, with a binding energy of 0.26 eV. Evidently this binding energy is low enough to lead to easy ionization of the polaron and the observation of p-type conductivity in Sr-doped GTO [35]. Strontium on a Ti site behaves similarly to Sr_{Gd}, with a (−1/0) transition level at 1.04 eV and the neutral charge state corresponding to a small polaron on a nearby Ti site, but with a significantly higher formation energy.

B. Hydrogen

The hydrogen interstitial can occur in two charge states. In the +1 charge state (essentially a proton) it bonds to an O atom, with a H-O bonding state resonant in the O $2p$ band, while in the −1 charge state it bonds to a Ti atom, introducing a H-Ti bonding state 1.33 eV above the O $2p$ band. The (+1/−1) transition level occurs at 1.12 eV (Fig. 6). Note that this is the first example we have encountered where a "true" charge-state transition level occurs, i.e., a transition that is truly associated with a change in the electronic structure of the defect center (including even a change in atomic structure, in this case), as opposed to merely binding a polaron to the center.

C. Carbon

Carbon substituting on an oxygen site (C_O) bonds with the two nearby Ti atoms, with slightly smaller Ti-C bond lengths (1.94 Å) than the comparable Ti-O bonds in the bulk (2.02 Å), which necessitates a larger Ti-C-Ti bond angle (150.3°) than the bulk Ti-O-Ti angle (140.4°). It introduces states between the O $2p$ band and the LHB; a spin-polarized pair of Ti-C bonding states (1.88 eV and 2.01 eV above the O $2p$ band), and four C lone-pair states (spin up states 1.93 eV and 2.17 eV above the O $2p$ band, and spin-down states at 2.09 eV and 2.34 eV). Since carbon is nominally a double acceptor when placed on the oxygen site, the "natural" charge state would be −2; Fig. 6 shows that this charge state only occurs when the Fermi level is very high in the gap. In the −1 and neutral charge states, one or two holes are bound to the center. Figure 7 illustrates that in the neutral charge state, a polaron is localized on each of the Ti atoms bonded to C. The polarons are strongly bound to the center, as indicated by the high values of the transition level: at 1.30 eV for (0/−1) and 1.84 eV for (−1/−2) (Fig. 6). C_O is the carbon-related defect with the lowest formation energy for both limits of chemical potentials.
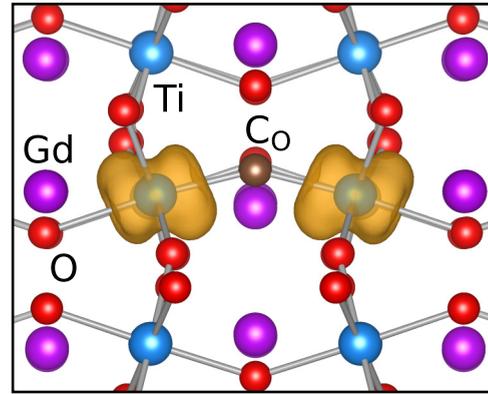
FIG. 7. Charge density of the small hole polaron states for C_O^0, with the isosurface set to 10% of the maximum value.

The carbon interstitial bonds with a substitutional O atom in a dumbbell configuration, similar to O_i. The O atom is significantly displaced from its substitutional site, increasing the distortion of the Ti-O-Ti bond angle. The interstitial introduces four spin-polarized C states above the O $2p$ band (1.81 eV and 2.33 eV above for spin-up, and 2.00 eV and 2.67 eV for spin-down). Similar to O_i, the −2 charge state is expected to be the natural charge state for C_i. It turns out that the Fermi level would need to be pushed very high (into the UHB) to achieve this charge state: the (−1/−2) level is at 2.09 eV. The (0/−1) transition level occurs at 1.15 eV (Fig. 6). In the −1 and neutral charge states, one or two polarons are bound to the defect center. C_i has high formation energies.

Carbon has four valence electrons and therefore might be expected to form a good "chemical match" when substituting on the Ti site; however, its size is significantly smaller, and the C atom moves off-site to form two 1.35 Å C-O bonds. For this bonding configuration of C_{Ti} we observe a doubly occupied C state 2.14 eV (spin-up) and 2.23 eV (spin-down) above the O $2p$ band. The −1 charge state is the "natural" charge state for this defect. Forming the 0 charge state leads to the formation of a hole polaron, with (−1/0) transition level at 1.07 eV (Fig. 6). We note that the formation energy of C_{Ti} is quite high; this is mainly due to the chemical potential of Ti being high to maintain stability of GTO (Fig. 2), which suppresses incorporation of impurities on the Ti site.

Carbon on a Gd site moves off-site and forms a 1.30 Å C-O bond. It introduces a spin-polarized C state (spin-up 0.15 eV above the O $2p$ band and spin-down 2.11 eV above). Its "natural" charge state is −3, and for the higher charge states polarons are localized on the nearby Ti atoms. The transition levels are at 0.84 eV (0/−1), 1.09 eV (−1/−2), and 1.87 eV (−2/−3) (Fig. 6). The formation energy of C_{Gd} is again high, for the same reasons related to chemical potentials as mentioned above for C_{Ti}.

V. DISCUSSION

A. Formation energies, transition levels, and binding of hole polarons

For the native defects Fig. 3 shows that under oxygen-rich conditions ($\mu_O = -3.61$ eV) the cation vacancies (V_{Ti} and

V_{Gd}) have the lowest formation energies, and under oxygen-poor conditions ($\mu_O = -5.25$ eV) oxygen vacancies (V_O) and Gd antisites (Gd_{Ti}) have the lowest formation energies. From Fig. 6 we see that among the C-related defects C_O has by far the lowest formation energy.

For all the studied defects except H_i, *all* the charge transition levels represent the addition/removal of a small hole polaron. The polaron-related transition levels range from 0.58 eV [(+1/0) level for Ti_{Gd}] to 1.87 eV [(−2/−3) level for C_{Gd}]. Energies higher than the 0.55 eV (+1/0) transition level for the polaron in bulk GTO indicate that the polaron has a finite binding energy to the defect center. In the case of the oxygen vacancy or the antisites, where the defect center itself is neutral, these binding energies are quite small (see Sec. III D); in the other cases, the defect centers themselves are negatively charged centers, leading to stronger binding of the hole polarons.

B. Optical properties

In previous work, we investigated the impact of small hole polarons on optical absorption [29]. The transition corresponding to the excitation of a small hole polaron to a delocalized hole state is shown in the configuration coordinate diagram in Fig. 8(a). The strain energy E_S is the energy difference between GTO in its equilibrium configuration and in the configuration corresponding to a small polaron, and the polaron self-trapping energy E_{ST} is the energy difference between the delocalized and localized hole in their relaxed atomic configurations.

Regarding the role played by small hole polarons in luminescence, an electron excited to the UHB could recombine with a small hole polaron. For a polaron in bulk GTO we calculate the peak of this emission to occur around 0.8 eV, as illustrated in Fig. 8(b). Since the defects introduce polaron transition levels that are higher than the bulk self-trapping energy $E_{ST} = 0.55$ eV (i.e., the polaron is more strongly bound), the 0.8 eV constitutes an upper limit on the optical emission energy E_e (assuming that the strain energy E_S is not significantly affected by the proximity of the polaron to the defect). However, defect-related transitions at such low energies are more likely to be nonradiative than radiative [36].

C. Defects as electron traps

GTO acts as the barrier layer that confines the 2DEG at STO/GTO interfaces [4]; it is therefore of interest to investigate the potential impact of defects on electron trapping. This could affect the performance of field effect transistors [37] and also of novel devices that would be based on tunneling through the GTO layer [38]. In the latter, electrons would tunnel between the 2DEG subbands at the interface and the subbands at another interface (in an STO/GTO/STO heterostructure) or a metal contact. In both cases tunneling electrons could be trapped/detrapped at defects in GTO. It is therefore important to assess the alignment of the charge-state transition levels in GTO with the band structure of the STO.

Figure 9 shows this alignment for the defects in GTO with a low formation energy, using the previously calculated band offset between GTO and STO [39]. In the "flat-band" diagram
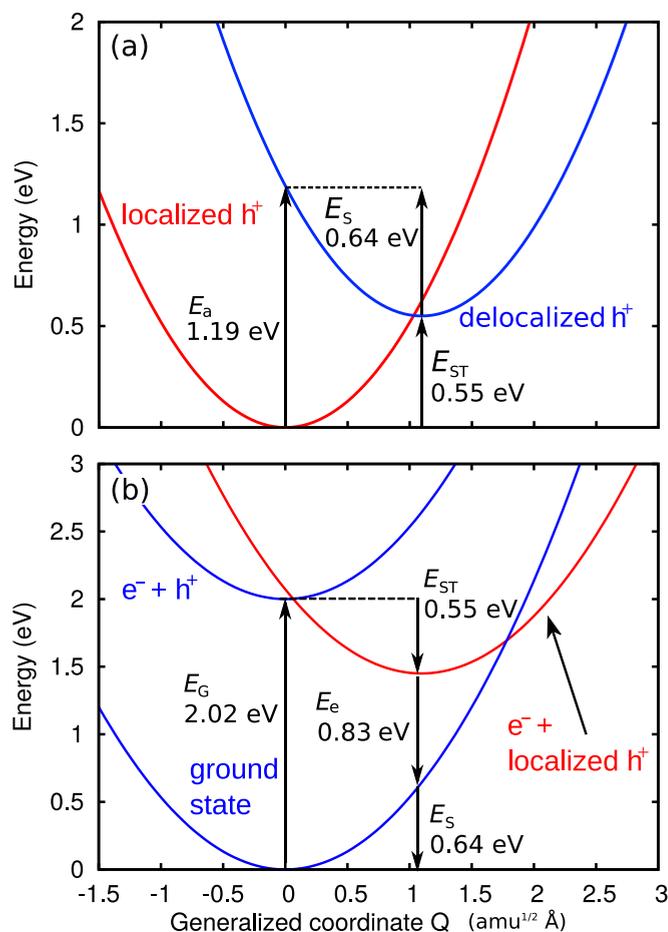
FIG. 8. Configuration coordinate diagrams (as calculated in Ref. [29]) for (a) the optical excitation of a hole from a localized to a delocalized state and (b) the recombination of an electron with a localized hole (small polaron). E_a is the absorption energy, E_G is the band-gap energy, E_{ST} the polaron self-trapping energy, E_e the optical emission energy, and E_S is the lattice energy cost (strain energy).

of Fig. 9, all transition levels (except that associated with a hole polaron in the bulk) are above the STO conduction-band minimum (CBM). However, in an actual heterostructure
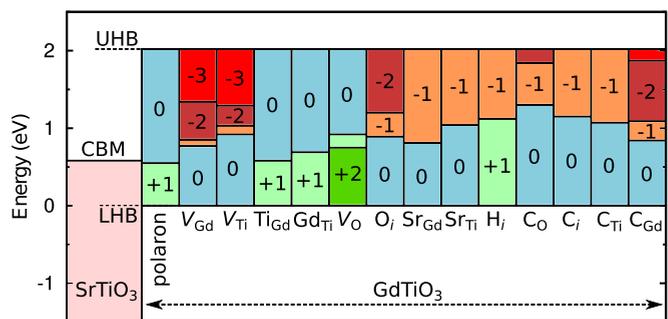
FIG. 9. Band alignment between STO and GTO, with positions of charge-state transition levels for native defects and impurities shown within the GTO gap. The zero of energy is set to the top of the GTO valence band (LHB), and the conduction-band minimum (CBM) of STO is indicated.

there will be band bending at the interface associated with the presence of the 2DEG in the GTO, thus raising the energy of the tunneling electrons. This band bending has been predicted to be as large as 1 eV [40], meaning that the highest Fermi level position would be about 1.6 eV above the GTO LHB. The application of a voltage to control the tunneling process may also lower the energy of the transition levels relative to the tunneling electrons. Taken together, this means that the tunneling electrons may line up in energy with the defect-related trapping levels.

To assess the impact of defects on leakage currents or on tunneling through a GTO barrier layer, we consider trapping/detrapping processes based on the formalism outlined by Fowler *et al.* [41], which has previously been applied to study leakage currents in SiO_2 [42]. Within this methodology, tunneling processes are approximated as Franck-Condon transitions, with atomic relaxation occurring after charge-state switching. Thus we define the "charge-state switching level" for trapping by adding the strain energy to the thermodynamic transition level [since this strain energy will be gained back only *after* the transition takes place, similar to the absorption event in Fig. 8(a)]. Similarly, the level for detrapping is defined by subtracting the strain energy from the thermodynamic transition level [since the system will subsequently relax to the final state, lowering its energy by this amount of strain energy, similar to the emission event in Fig. 8(b)]. Note that the strain energies for trapping and for detrapping are different.

As discussed in Sec. III and IV, for all point defects except the hydrogen interstitial the transition levels are associated with small hole polarons. Therefore, we first illustrate these concepts for the case of a polaron in the bulk, and subsequently discuss how the binding of the polaron to a defect would affect the charge-state switching levels.

A hole polaron by itself gives a $(+/0)$ transition level at 0.55 eV, and may recombine with a tunneling electron. This $(+/0)$ transition corresponds to occupying the hole polaron state with an electron. This is similar to what happens when a small hole polaron transitions to a delocalized state via optical absorption [as illustrated in Fig. 8(a)]: in that case, an electron at the top of the LHB is excited to occupy the polaron state, leaving behind a delocalized hole. The energy E_a required for the optical absorption process is the sum of the polaron self-trapping energy $E_{ST} = 0.55$ eV and the strain energy $E_S = 0.64$ eV. In the case of electron tunneling, the electron would therefore need to be injected at an energy 0.55 eV + 0.64 eV = 1.19 eV above the LHB, as illustrated in Fig. 10(a). The charge-state switching level for electron trapping is thus at 1.19 eV. After the electron has filled the polaron state, lattice relaxation occurs (through phonon emission), and the final state corresponds to the perfect GTO lattice—i.e., there is no detrapping level in this case.

Now we examine the electron-trapping process in the presence of defects. To illustrate this we use the 1.30 eV $(0/-)$ transition level for C_O, the lowest-energy C-related defect. Since the Fermi level is likely to lie below 1.30 eV, C_O is initially in the neutral charge state and two polarons are localized on the nearest-neighbor Ti atoms (C_O^0). The difference in energy between C_O^- in its equilibrium configuration and C_O^- in the configuration of C_O^0 (E_{S1}) is 0.38 eV. Adding this
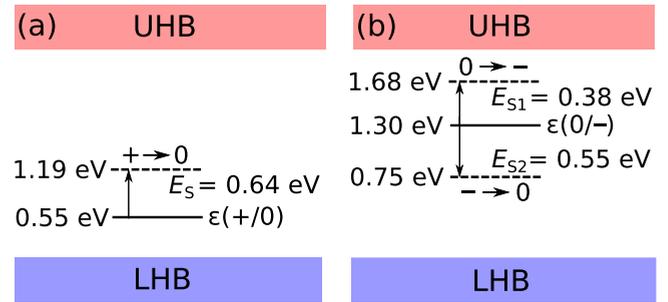
FIG. 10. Thermodynamic transition levels and charge-state switching levels for trapping/detrapping of an electron, for (a) the $(+1/0)$ transition for a polaron in bulk GTO and (b) the $(0/-1)$ transition for C_O. The arrows indicate a transition in which the atomic configuration is kept fixed to that of the initial state (unlike the thermodynamic transition levels, for which the atomic configuration of the final state is relaxed). $E_{S(1,2)}$ are the relaxation energies between the two charge states.

strain energy to the transition level gives a 1.68 eV charge-state switching level for the $0 \rightarrow -$ trapping process [Fig. 10(b)].

After an electron is trapped, C_O is in the negative charge state, and the defect will relax to its ground-state atomic configuration. We now address whether the electron would remain trapped on the defect, or be able to tunnel out. To remove the electron, a transition to the neutral charge state would need to occur. Again, the thermodynamic transition level is at 1.30 eV, but now we need to take into account the strain energy corresponding to the difference in energy between C_O^0 in its equilibrium configuration and C_O^0 in the configuration of C_O^- (E_{S2}). This energy, E_{S2}, is 0.55 eV. Subtracting this strain energy from the transition level gives a charge-state switching level of 0.75 eV for the $- \rightarrow 0$ detrapping process, as indicated in Fig. 10(b). Empty states would need to be available at that energy on the "exit" side of the barrier in order for the electron to be able to escape from the C_O trap.

For the range of possible Fermi levels, which we estimated above to be between 0.6 to 1.6 eV, multiple defects occur in charge states that stabilize small hole polarons. These defects may act as trapping centers once a voltage is applied: an electron tunnels into the defect, fills a hole polaron, and the defect switches to another charge state. For this electron to become detrapped, there must be an empty state available on the other side of the junction. It is evident from Fig. 10(b) that for this criterion to be satisfied, the voltage swing applied to the device must therefore be greater than the sum of the strain energies associated with the charge-state switching level; in the example of C_O $(0/-)$, this would be 0.38 eV + 0.55 eV = 0.93 eV. Assuming that the strain energies are similar for all the defects (except H_i), since all the transition levels involve small polarons, we conclude that defects may only contribute to tunneling for applied voltage swings greater than about 0.9 V. For smaller applied voltage swings, there are no empty states available on the other side of the junction, and the defect level may act as a trapping center, i.e., electrons would be trapped on the defect without the possibility of detrapping; this would lead to charging of the GTO layer, which could be detrimental to device operation.

VI. SUMMARY

We have investigated the electronic and optical properties of intrinsic and extrinsic point defects in GTO using hybrid density functional theory. Results for formation energies of native defects are summarized in Fig. 3. It should be noted that this figure should be interpreted somewhat differently from the usual case of semiconductors or band insulators [22]: the kinks in the curves, which define the positions of the defect levels according to Eq. (2), do *not* correspond to adding or removing electrons from electronic states within the band gap here; rather, they represent the formation of polarons in the vicinity of the defect, while the center of the defect remains in the charge state in which the bonding states are fully occupied. The same is true for all of the impurities in Fig. 6, except interstitial H. Among the native defects, the cation vacancies have the lowest formation energies under oxygen-rich conditions and the oxygen vacancy under oxygen-poor conditions. Among candidate impurities, Sr_{Gd} is an acceptor with low formation energy, H_i has a level in the middle of the gap, and C_O has the lowest energy among C-related defects.

The transition levels for all defects (except H_i) are related to small hole polarons. In the bulk, the $(+/0)$ transition level for a polaron is at 0.55 eV. The transition levels for defects are higher in energy because of the binding of the polaron to the defect. The defects can act as electron traps or sources of leakage current in GTO barrier layers in devices. We find that defects would only act as tunneling centers (enabling trapping and detrapping of electrons) if applied voltage swings are greater than about 0.9 V. Several of the defects can lead to electron trapping and charging of the GTO layer.

[1] M. Imada, A. Fujimori, and Y. Tokura, Rev. Mod. Phys. **70**, 1039 (1998).

[2] H. D. Zhou and J. B. Goodenough, J. Phys. Condens. Matter **17**, 7395 (2005).

[3] N. F. Mott, Proc. Phys. Soc. London Sect. A **62**, 416 (1949).

[4] P. Moetakef, T. A. Cain, D. G. Ouellette, J. Y. Zhang, D. O. Klenov, A. Janotti, C. G. Van de Walle, S. Rajan, S. J. Allen, and S. Stemmer, Appl. Phys. Lett. **99**, 232116 (2011).

[5] S. Stemmer and S. J. Allen, Annu. Rev. Mater. Res. **44**, 151 (2014).

[6] D. A. Crandles, T. Timusk, J. D. Garrett, and J. E. Greedan, Physica C **201**, 407 (1992).

[7] P. Moetakef, D. G. Ouellette, J. Y. Zhang, T. A. Cain, S. J. Allen, and S. Stemmer, J. Cryst. Growth **355**, 166 (2012).

[8] A. Alkauskas, P. Broqvist, and A. Pasquarello, Phys. Status. Solidi B **248**, 775 (2011).

[9] F. Oba, A. Togo, I. Tanaka, J. Paier, and G. Kresse, Phys. Rev. B **77**, 245202 (2008).

[10] P. Deák, B. Aradi, T. Frauenheim, E. Janzén, and A. Gali, Phys. Rev. B **81**, 153203 (2010).

[11] J. L. Lyons, A. Janotti, and C. G. Van de Walle, Phys. Rev. Lett. **108**, 156403 (2012).

[12] A. Alkauskas, J. L. Lyons, D. Steiauf, and C. G. Van de Walle, Phys. Rev. Lett. **109**, 267401 (2012)

[13] J. He and C. Franchini, Phys. Rev. B **86**, 235117 (2012).

[14] B. Himmetoglu, A. Janotti, L. Bjaalie, and C. G. Van de Walle, Phys. Rev. B **90**, 161102(R) (2014).

[15] J. Heyd, G. E. Scuseria, and M. Ernzerhof, J. Chem. Phys. **118**, 8207 (2003).

[16] J. Heyd and G. E. Scuseria, J. Chem. Phys. **121**, 1187 (2004).

[17] G. Kresse and D. Joubert, Phys. Rev. B **59**, 1758 (1999).

[18] G. Kresse and J. Furthmüller, J. Comput. Mater. Sci. **6**, 15 (1996).

[19] J. Paier, M. Marsman, K. Hummer, G. Kresse, I. C. Gerber, and J. G. Angyán, J. Chem. Phys. **124**, 154709 (2006).

[20] P. Rivero, I. P. R. Moreira, G. E. Scuseria, and F. Illas, Phys. Rev. B **79**, 245129 (2009).

[21] L. Bjaalie, A. Verma, B. Himmetoglu, A. Janotti, S. Raghavan, V. Protasenko, E. H. Steenbergen, D. Jena, S. Stemmer, and C. G. Van de Walle, Phys. Rev. B **92**, 085111 (2015).

[22] C. Freysoldt, B. Grabowski, T. Hickel, J. Neugebauer, G. Kresse, A. Janotti, and C. G. Van de Walle, Rev. Mod. Phys. **86**, 253 (2014).

[23] C. Freysoldt, J. Neugebauer, and C. G. Van de Walle, Phys. Rev. Lett. **102**, 016402 (2009).

[24] C. Freysoldt, J. Neugebauer, and C. G. Van de Walle, Phys. Status Solidi B **248**, 1067 (2011).

[25] M. W. Chase Jr., *NIST-JANAF Thermochemical Tables*, 4th ed., J. Phys. Chem. Ref. Data (NIST, Washington, DC, 1998), Monograph 9.

[26] *CRC Handbook of Chemistry and Physics*, W. M. Haynes, 95th ed. (CRC Press, Boca Raton, 2014).

[27] K. B. Helean, S. V. Ushakov, C. E. Brown, A. Navrotsky, J. Lian, R. C. Ewing, J. M. Farmer, and L. A. Boatner, J. Solid State Chem. **177**, 1858 (2004).

[28] K. Jacob and G. Rajitha, J. Chem. Thermodyn. **43**, 51 (2011).

[29] L. Bjaalie, D. G. Ouellette, P. Moetakef, T. A. Cain, A. Janotti, B. Himmetoglu, S. J. Allen, S. Stemmer, and C. G. Van de Walle, Appl. Phys. Lett. **106**, 232103 (2015).

[30] A. Janotti, J. B. Varley, M. Choi, and C. G. Van de Walle, Phys. Rev. B **90**, 085202 (2014).

[31] L. Weston, A. Janotti, X. Y. Cui, C. Stampfl, and C. G. Van de Walle, Phys. Rev. B **89**, 184109 (2014).

[32] M. Choi, A. Janotti, and C. G. Van de Walle, Phys. Rev. B **88**, 214117 (2013).

[33] T. A. Cain, P. Moetakef, C. A. Jackson, and S. Stemmer, Appl. Phys. Lett. **101**, 111604 (2012).

[34] D. G. Ouellette, P. Moetakef, T. A. Cain, J. Y. Zhang, S. Stemmer, D. Emin, and S. J. Allen, Sci. Rep. **3**, 3284 (2013).

[35] T. A. Cain and P. Moetakef, Thin Solid Films **583**, 129 (2015).

[36] A. Alkauskas, Q. Yan, and C. G. Van de Walle, Phys. Rev. B **90**, 075202 (2014).

[37] M. Boucherit, O. Shoron, C. A. Jackson, T. A. Cain, M. L. C. Buffon, C. Polchinski, S. Stemmer, and S. Rajan, Appl. Phys. Lett. **104**, 182904 (2014).

[38] S. Raghavan, S. J. Allen, and S. Stemmer, Appl. Phys. Lett. **103**, 212103 (2013).

[39] L. Bjaalie, B. Himmetoglu, L. Weston, A. Janotti, and C. G. Van de Walle, New J. Phys. **16**, 025005 (2014).

[40] H. Peelaers, K. Krishnaswamy, L. Gordon, D. Steiauf, A. Sarwe, A. Janotti, and C. G. Van de Walle, Appl. Phys. Lett. **107**, 183505 (2015).

[41] W. B. Fowler, J. K. Rudra, M. E. Zvanut, and F. J. Feigl, Phys. Rev. B **41**, 8313 (1990).

[42] P. E. Blöchl and J. H. Stathis, Phys. Rev. Lett. **83**, 372 (1999).